Proceedings of Global Power and Propulsion Society
ISSN-Nr: 2504-4400
GPPS Xi'an21
18th – 20th October, 2021
www.gpps.global

GPPS-TC-2021-0117

Research On Aero Engine Intake Distortion Based On 3D CFD Full Engine Simulation

Yibing Xu
Tsinghua University
xyb18@mails.tsinghua.edu.cn
Beijing, P.R.China

Wantong Wu
Tsinghua University
wwt15@mails.tsinghua.edu.cn
Beijing, P.R.China

Wei Liu
Tsinghua University
lw18@mails.tsinghua.edu.cn
Beijing, P.R.China

Ying Piao
Tsinghua University
piaoying@mail.tsinghua.edu.cn
Beijing, P.R.China

ABSTRACT

Intake distortions have large impacts on the performance of aero engines, and the investigations on intake distortions are in great need. Note that the component-decoupled simulations tend to break the constraint of power matching between compressor/turbine, which is key to understanding the underlying complicated process of intake distortions. In the present work, a steady-state three-dimensional component-coupled full engine simulation for a micro-turbojet engine, in which the aerodynamic/power matching is guaranteed, was employed to study the impacts of intake distortion on the engine operating state. The coupled/decoupled simulations are first applied to the states without intake distortion to reveal the advantage of coupled scheme. For intake distortion conditions, two typical adjustment strategies are adopted respectively to make the engine stable at rebalanced operating points, and the performance of the compressor in conjunction with the thrust of the full engine is analysed in detailed. The analytical results show that the matching problems induced by intake distortions are systematically demonstrated by the component-coupled scheme.

INTRODUCTION

The inlet non-uniform flow, known as "intake distortion", is inevitable in the actual working process of the aero engine. Different types of intake distortion may occur for different reasons, such as ingestion of boundary layers, break-away flow at intake lips, or wakes from stalled wings (Reid, 1969). Previous studies about intake distortion almost focused on the front components of engines (Cousins.et al, 1993; Pecinka.et al, 2015), reporting that the compressor performance was always deteriorated. While for the engine designers, the full engine performance is the ultimate target parameter. The research on the response of the engine to intake distortions will contribute to developing new engines and the high stability distortion tolerant control system (Delaat.et al, 1998).

Generally, rig experiment with intake distortion device is a feasible method to study the intake characteristics of the engine (Naseri et al, 2018), but the cost is considerable. As for the numerical simulation methods, multiple segment parallel compressor model (Mazzawy, 1977) was extended to assess the effects of circumferential intake distortion on the the full engine (Yan.et al, 2015). Since each segment is based on low dimensional flow assumptions, it's not applicable for complex intake distortion condition. "Mini-maps" zooming method (Turner.et al, 2004) is an effective method to calculate the performance of the full engine, which combined three-dimensional computational fluid dynamics (3D CFD) simulation of components and 0D cycle simulation of the engine. But it is still an one-way coupled method, and more importantly, the mini-maps of each components under the given intake distortion is usually unavailable. The 3D CFD full engine simulation method might be a batter way to predict the effects of complex intake distortion on the full engine, and it has been rapidly developed in recent years. The potential of this method to compute engine performance at design points has been verified in some studies (Wang, 2013; Krivcov.et al, 2014).

In this paper, 3D CFD full engine simulation was implemented to study the intake distortion of aero-engine with power balance automaticly. It is proved that only taking aerodynamic/power matching into consideration, could 3D CFD full engine simulation be used as a potential tool for engine design or for drawing up the engine control strategy.

METHODOLOGY

Modeled Engine Basic Data

The KJ66 micro turbojet engine (MTE) with public data is selected as the test case, which is compact designed to a small size. It is composed of three core components:single-stage centrifugal compressor, single-stage axial flow turbine, and an annular combustor. Considering the size of the combustor, vaporizing injector pipes are mounted in it to get the well-proportioned mixture of fuel and air rapidly. Several versions of KJ66 can be found in previous studies, with slightly difference in their performance. In this paper, a new typical one-spool micro turbojet engine (New KJ66 MTE, see Figure 1) derived from the dual-spool KJ66 micro gas turbine (MGT) (Teixeira.et al, 2018) has been studied in detail.

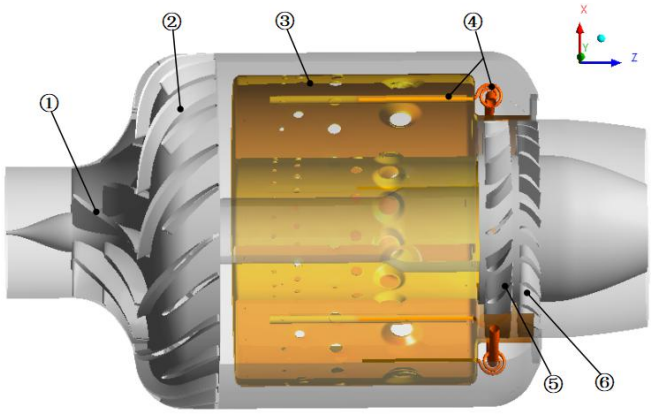

Figure 1. The Layout of the New KJ66 MTE：1)Impeller; 2) Diffuser; 3)Combustion chamber; 4)Vaporizing burner; 5)Turbine guide vane; 6)Turbine rotor

Table 1 shows the main configuration parameters of the New KJ66 MTE. As mentioned in the previous article, at the steady operation point, the power (or torque) of impeller and turbine rotor should be in balance, and when the rotor spins at 80000 rpm, the vaporized kerosene should be injected from the vaporizing injector pipes at axial velocity of -125m/s. For this New KJ66 MTE, the design rotation speed was pitched on 80000 rpm, and the velocity of fuel (kerosene $C_{12}H_{23}$) gas should be fine tuned around -125m/s. And the inflow Reynolds number at the engine design point is about 6×10^5.

Table 1.The main configuration parameters of the redesigned New KJ66 MTE

Parameters	Units	Data
Length	mm	240
Maximum diameter	mm	108
Turbine rotor diameter	mm	66
Impeller(splitter) blade count	-	6（6）
Diffuser(splitter) blade count	-	12（12）
Vaporizing injector pipes count	-	6
Turbine guide vane count	-	18
Turbine rotor blade count	-	24
Engine weight	kg	0.93

Meshing and Flow Solver

Considering the periodicity of all components, the computational domain only encompassed one periodic passage. For the combustion chamber, a 60°sector containing one vaporizing injector pipe was zoned for meshing the unstructured tetrahedral grid. And the structured hexahedral grid was generated for the blade rows of compressor and turbine. The tip

clearance of the rotor blade was set as 1% of the blade height, and the clearance between stator and hub was ignored. All tip clearance was filled with the H-type grids. In order to accurately solve the turbulent flow near the wall, the grid thickness of the first layer near the wall was set as 0.01 mm to ensure that the Y-plus met the requirements of the specific turbulence model (The maximum value of the Y-plus on all blades' wall is 9.64). The entire grid had 8.1 million elements in total, and contained about 0.8 million elements for each blade row. A view of the grid on the solid walls of the entire computation domain and several enlarged view of the grid detials for components are presented in Figure 2.

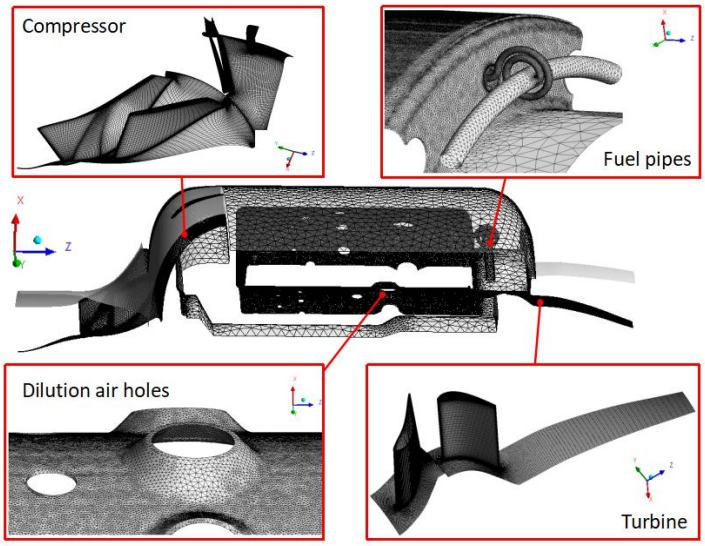

Figure 2. The Grid of the computation domain for the New KJ66 MTE

In this paper, all components were assembled for the full engine simulation by ANSYS CFX using steady RANS solver. As a pressure-based coupled solver, it can be applied to simulate the compressible flow in turbomachinery and constant-pressure combustion in combustion chamber. The RANS equation was closured by k-epsilon turbulence model with scalable wall functions. The working medium of the full engine was the mixture of air, gaseous fuel and their combustion products. The spatial distribution of the specific component mass fractions were obtained by solving the relevant equations. The combustion flow was simulated with EDM (Eddy Dissipation Model) and the chemical reactions were calculate using the one-step reaction mechanism (Westbrook.et al, 1984). Meanwhile, the thermal radiation was modeled by P1 model.

For the boundary conditions, the total temperature and total pressure were given at the inlet and the environmental static pressure was given at the outlet. The lateral boundary of the calculation domain was set as a rotating periodic boundary, and the wall area was given as an adiabatic wall without slip. The mixing-plane method was adopted to deal with the rotor-stator interfaces.

When the calculation converged at the stable operation points, the numerical residual should be stabilized at a low level. Moreover, the evolution of the torque deviation between compressor impeller and turbine rotor should be checked during the computation process to ensure that it was stable and balanced, just like the requirements for the mass flow. For this purpose, the error of mass flow and torque are defined respectively as follows:

$$e_{mass} = \frac{m_0 + m_{fuel} - m_9}{m_2}. \qquad (1)$$

$$e_{torque} = \frac{Tq_T - Tq_C}{(Tq_T + Tq_C)/2}. \qquad (2)$$

The parameters at the key interface are marked with numeral subscript as customary, the subscript 0 stands for the inlet and subscript 9 for outlet.

RESULTS AND DISCUSSION

Simulation for Clean Intake

In the ideal state, the engine works at an uniform ambient atmosphere. Here, an uniform ambient total quantities (total temperature 293K and total pressure 101325Pa) and the inflow with specified axial velocity direction were imposed at the engine inlet. The outlet boundary was set to an estimated static pressure about 101325Pa. For the the design operation point with the 80000rpm rotation speed and -125m/s axial velocity of the fuel gas, the calculation of full engines was well converged at a steady state after 1000 iterations.

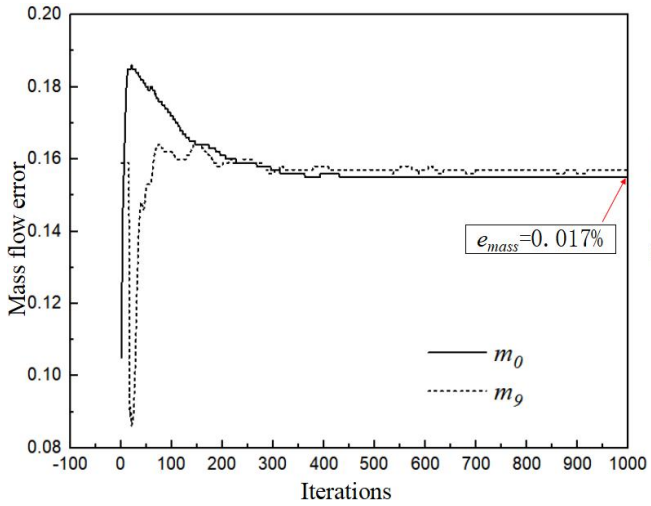

Figure 3(a). The convergence history of the mass flow at the engine inlet and outlet

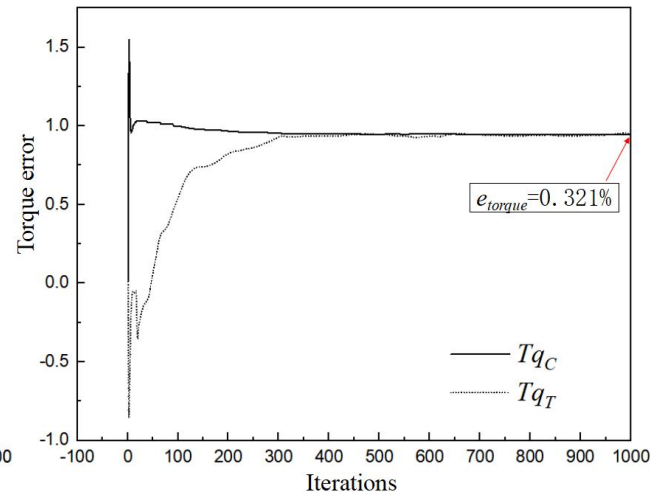

Figure 3(b). The convergence history of the torque of the compressor impeller and turbine rotor.

Figure 3 shows the convergence history of mass flow and the torque. It is obviously that the mass flow and torque were all stabilized, and the error of them dropped to a fairly low level. That means the calculation of the flow field converged well and the power of the coaxial components was balanced. Figure 4-(a) is the static temperature distribution in the full engine computation domain with volume rendering. Figure 4-(b) is the meridional views of the computation domain along with static temperature distribution, which marked with circumferential average quantities and the performance parameters at the key interfaces.

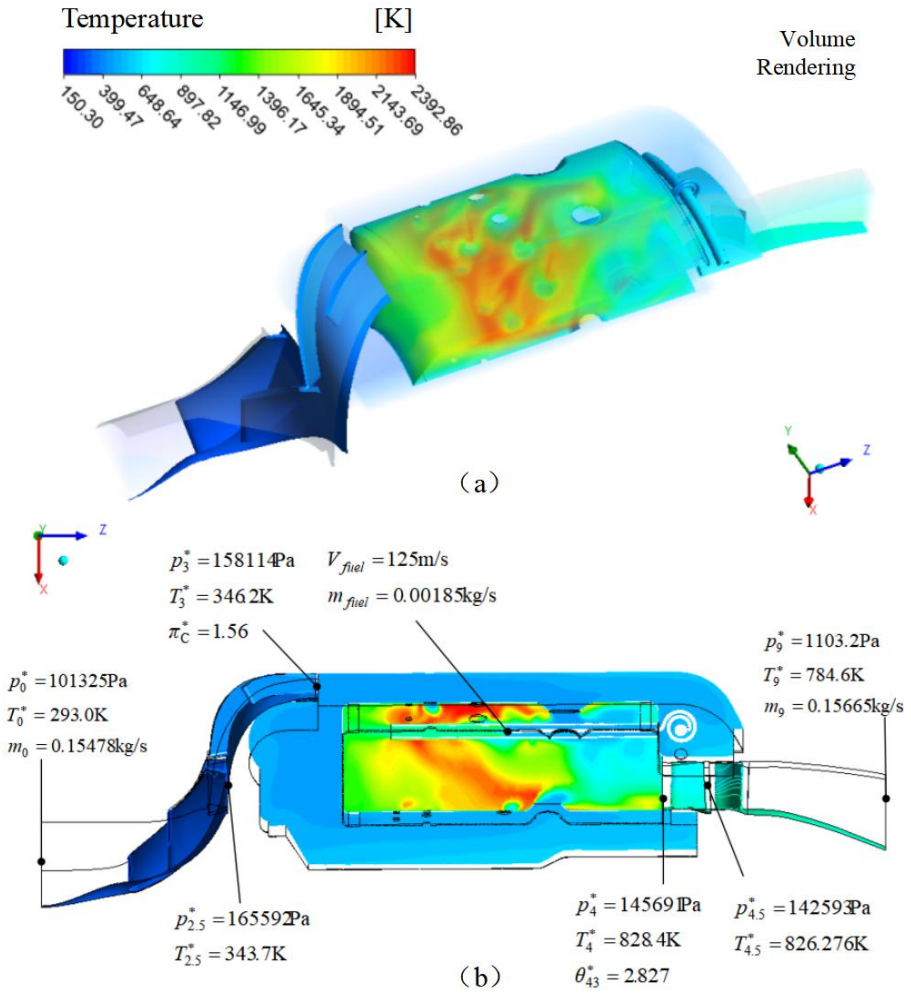

Figure 4 The static temperature distribution of the converged flow filed

The results show that the maximum static temperature is 2392.86K for the whole flow field, and the high temperature combustion zone is located in the inner chamber. The maximum static temperature of all the solid wall is 1269K, under the tolerable temperature of the common alloy materials.

In order to fully understand the performance of this New KJ66 MTE, the general characteristic map of compressor and the co-working line of the engine were acquired at four rotation speed by 3D CFD calculation, which are presented in Figure 5. All co-working points in this figure are power balanced states calculated by 3D CFD full engine simulation.

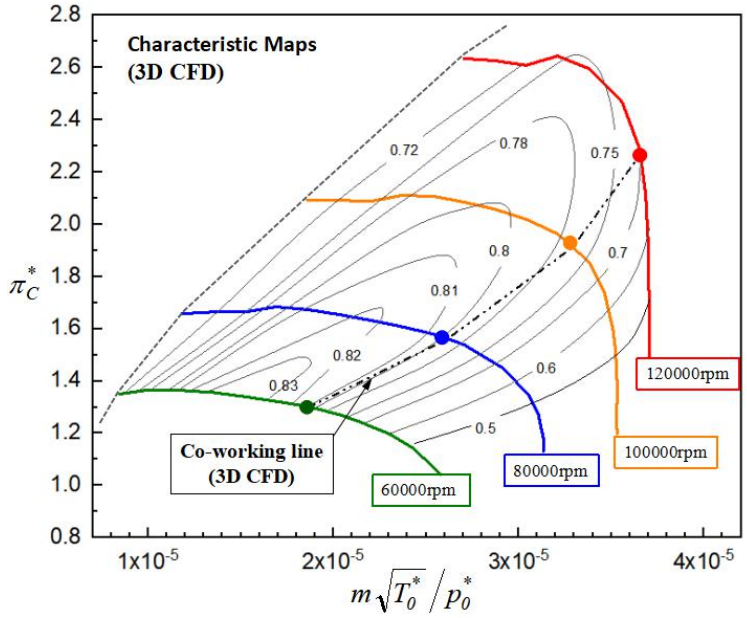

Figure 5 The general characteristic map with co-working line

Simulation for Distortion Intake

Non-uniform total pressure is a common type of inlet distortion. Radial non-uniform inlet distortion is an abstractly boundary conditions representing the real intake state to a certain extent. In this paper, two kinds of radial total pressure distortion intake (DI_A and DI_B) were detailed calculated to study the impacts on the performance of the engine. Compared to the clean intake (CI), only the total pressures on both sides of the inlet middle radius were increased or decreased by 10%. Figure 6 shows the total pressure at the engine inlet for this three inlet conditions.

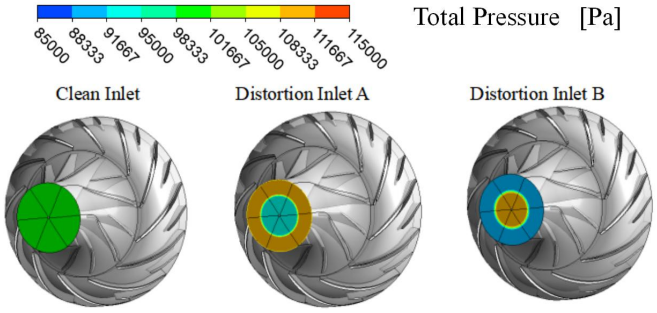

Figure 6 The total pressure at the engine inlet for three inlet conditions studied in this paper

Steady simulation of the full engine is generally used to predict the stable operating points. The computations of the distortion-intake case were restarted based on the convergent initial flow field of the clean-intake case. It is important to note that, once the intake distortion conditions was imposed, the power balance of the coaxial components based on the previous state would be broken. In order to achieve the new balanced operating points, some state parameters such as rotate speed and fuel flow needed to be adjusted. Two typical adjustment strategies were discussed to reach the new state:

1)Constant rotation speed strategy (Stg1): the rotation speed keeps constant ($n = 80000\text{rpm}$) while the velocity of fuel at the fuel inlet is adjusted;

2)Constant fuel flow strategy (Stg2):the velocity of fuel at the fuel inlet keeps constant ($V_{fuel} = -125\text{m/s}$) while the rotation speed is adjusted;

In the paper, the strategies Stg1 and Stg2 were tested for each distortion intake case.Take distortion intake conditions DI_A as an example, the convergence history of the torque based on the above two strategies are presented in Figure 7.

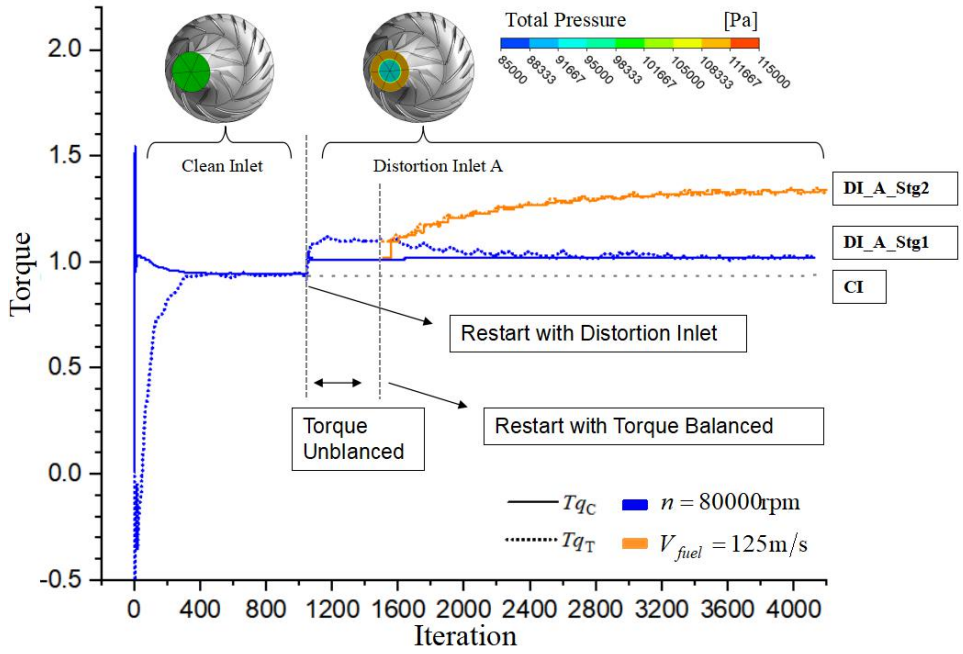

Figure 7 The convergence history of the torque based on two strategies(Stg1 andStg2)

As it's shown in the Figure 7, the torque deviation of the coaxial components can't drop to a reasonable range under pure CFD iterations. That is to say, only with the adjustment strategies of the engine state parameters, could the power or torque balance be achieved in CFD simulation, and the final convergence states were different at this two strategies.

Analysis of Influences

For the design rotation speed ($n = 80000$rpm), the influence of inlet distortion (DI_A and DI_B) on compressor characteristics was studied by individual components simulations. And based on the clean intake case (CI) of the full engines simulations at design rotation speed, other four distortion intake cases (DI_A_Stg1, DI_A_Stg2, DI_B_Stg1 and DI_B_Stg2) were implemented by component-coupled simulations. The calculation result of the above case are illustrated on the general characteristic map of compressor as Figure 8.

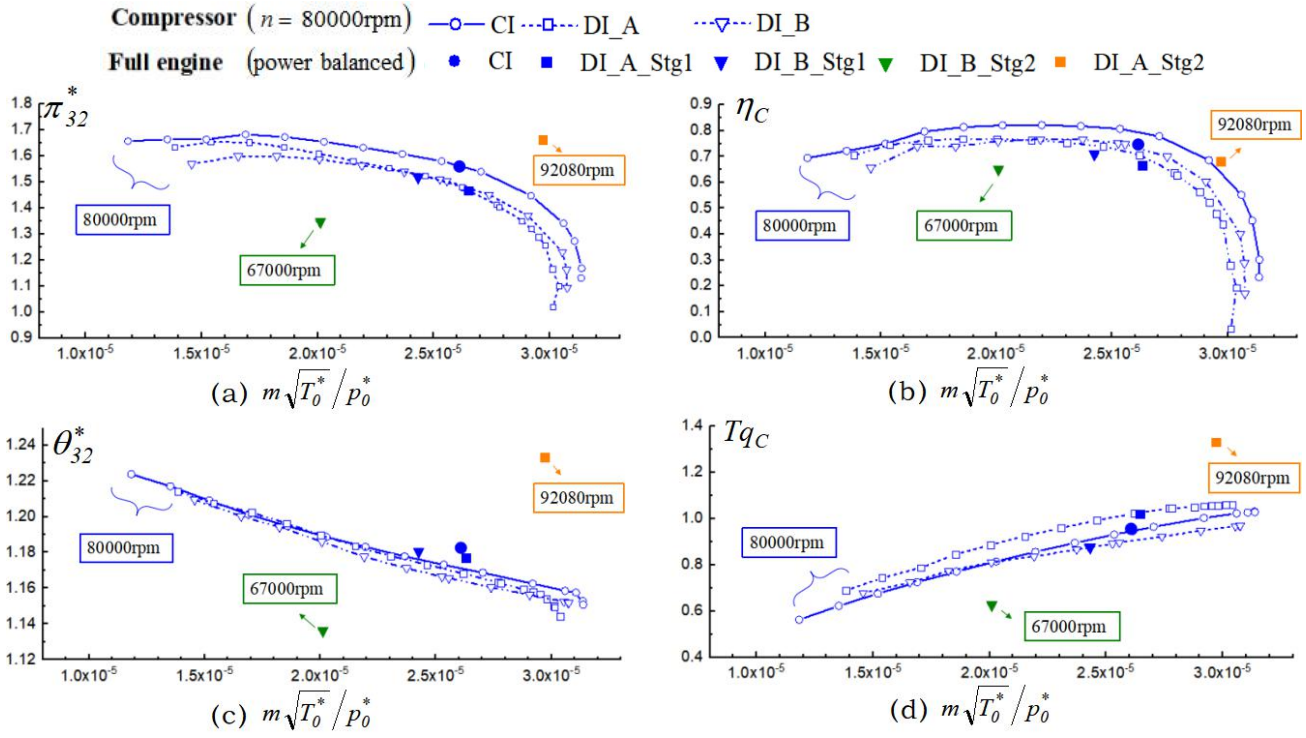

Figure 8 The basic parameters of compressor for the distortion-intake and clean-intake simulations

The calculation results of the individual compressor show that the aerodynamic parameters of the compressor, such as π_{32}^* , θ_{32}^* and η_C , descended similarly for different radial total pressure distortion intake DI_A and DI_B, while the torque variations under DI_A and DI_B were different. It can be seen form the Figure 8(d) that, at rotation speed 80000rpm, the torque of compressor Tq_C is greater in the entire flow rate range for DI_A inlet condition. But for DI_B inlet condition, Tq_C is greater than CI case in low flow rate and smaller in high flow rate range. This means that the rotor-dynamic balance might be more sensitive to the distortion intake than the aero-dynamic balance for this engine.

When the rotation speed is maintained at 80000rpm, the distinction of π_{32}^* and Tq_C between individual components simulations and full engines simulations is unobvious. However, in Figure8(c), the total temperature ratio of the the compressor is obviously improved under the full engine environments. This leads to a decrease of compressor efficiency, as shown in Figure8(b). The high temperature environment produced by the adjacent combustor may conduce to this difference between individual components simulations and full engines simulations.

According to the full engine simulation shown in Figure 8, constant rotation speed strategy (Stg1) had a slight influence on the parameters of the compressor and the engine, while constant fuel flow strategy (Stg2) caused significant changes. With strategy Stg2, the rotation speed and the mass flow rate of the new balanced operating points is following the the same trend of torque under distortion intake conditions.

As we know, intake distortion will affect the thrust of the engine. In this article, the thrust of the engine was calculated as a result parameter of the 3D CFD full engine simulations. The total thrust of the turbo-jet engine F_{thrust} is composed of momentum thrust F_m and pressure thrust F_p , which is defined as:

$$F_{thrust} = F_m + F_p = \left(m_9 V_9 - m_0 V_0 - m_{fuel} V_{fuel}\right) + \left(p_9 - p_0\right) A_9 . \qquad (3)$$

And from the definition (3), we know that the momentum thrust is determined by the velocity at the inlet and outlet, while pressure thrust is dominated by the static pressure. Figure 9 shows those thrusts under different intake conditions and adjustment strategies. Taking the clean intake case as the baseline, the non-dimensional variations of the velocity and static pressure are presented in Figure 10.

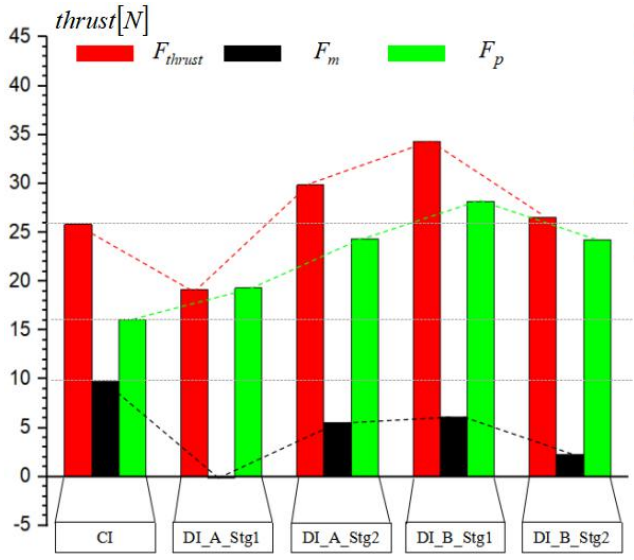

Figure 9. The thrust and its components under different intake and adjustment conditions .

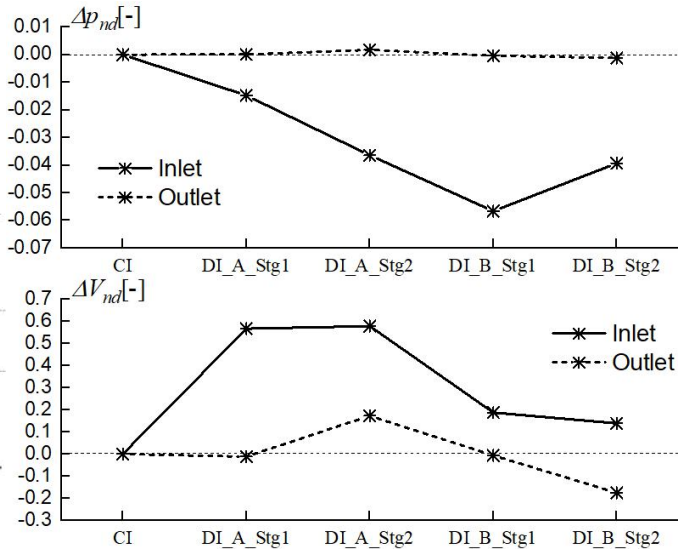

Figure 10. The non-dimensional variation of velocity and static pressure at the inlet and outlet.

It indicates that for this New KJ66 MTE, total thrust is mainly contributed by the pressure thrust. This probably result from the low flow mass rate of this micro turbo-jet engine. And considering the requirements of propulsive efficiency, the difference between V_9 and V_0 should not be very large. For the pressure thrust, although the non-dimensional variation of the static pressure is only a few hundredth, its effect is noticeable.

And as shown in the Figure 9 and10, the trend of the static pressure at the inlet is inversely correlated with the pressure thrust. This may be due to the static pressure boundary conditions imposed at the engine outlet. Other outlet boundary conditions may weaken this correlation.

In addition, the pressure thrust increases for each case under different distortion intake conditions, but the total thrust changes without obvious regulation. And it's difficult to maintain a constant thrust with simple adjustment strategy like constant rotation speed strategy or constant fuel flow strategy.

CONCLUSIONS

In this paper, the component-decoupled simulations for the compressor and the component-coupled simulations for the full engine were implemented through three-dimensional CFD method. The impacts of coupled/decoupled schemes on the simulation results for the compressors were discussed. It is shown that, compared with the decoupled scheme, the combustion chamber simulated with the coupled scheme provided a higher outlet temperature for the compressor, which dominates the deterioration of the compressor efficiency. As the static temperature of outlet boundary condition cannot be given adaptively in the decoupled scheme, it is difficult to avoid this aerodynamic matching problem.

Furthermore, the power balance of the coaxial components is proved to be influential for the steady three-dimensional CFD full engine simulation. In this work, the torque deviation between compressor impeller and turbine rotor is significantly smaller than the results in previous papers. This is due to the automatic torque balance iteration introduced to the CFD solving processes, which well ensured the power balance of the full engine steady simulations.

For the cases with intake distortions, the feasibility of two typical adjustment strategies used in simulation, constant rotation speed strategy and constant fuel flow strategy, were verified to achieve the new balanced operating points. These two typical adjustment strategies will make the engine work steadily at difference states providing different thrusts. To maintain a constant thrust under intake distortion, some more complex adjustment strategies should be imposed for this micro turbojet engine. This indicates that the three-dimensional CFD full engine simulation method used in this paper, is not only applicable to predict the off-design performance of the engine, but also can be used as a potential tool for drawing up the engine control strategy.

NOMENCLATURE

			Superscripts/Subscripts		
m	=	mass flow rate			
π	=	pressure ratio	$*$	=	stagnation quantities
θ	=	temperature ratio	nd	=	non-dimensional value
η	=	isentropic efficiency	C	=	compressor parameter
p	=	pressure	T	=	turbine parameter
T	=	temperature	*fuel*	=	parameter at fuel inlet
n	=	rotation speed	1	=	engine inlet
V	=	velocity	2	=	compressor inlet
F	=	thrust	3	=	compressor outlet
Tq	=	torque	4	=	combustor outlet
A	=	area	5	=	turbine outlet
e	=	error	9	=	engine outlet

REFERENCES

Cousins, W. T., Dalton, K. K., Andersen, T. T. & Bobula, G. A. (1993) Pressure and Temperature Distortion Testing of a Two-Stage Centrifugal Compressor. Journal of Engineering for Gas Turbines & Power, 116(3), 567-573.

Delaat, J., Southwick, R., Gallops, G. & Orme, J. (1998) The High Stability Engine Control (HISTEC) program - Flight demonstration phase, 34th AIAA/ASME/SAE/ASEE Joint Propulsion Conference and Exhibit.

Krivcov, A. V., Shabliy, L. S. & Baturin, O. V. (2014) Gas-Dynamic Modeling of Gas Turbine Engine Components Collaborative Workflow. Open Mechanical Engineering Journal, 8(1), 445-449.

Mazzawy, R. S. (1977) Multiple Segment Parallel Compressor Model for Circumferential Flow Distortion. Journal of Engineering for Gas Turbines & Power, 99(2), 288-296.

Naseri, A., Sammak, S., Boroomand, M., Alihosseini, A. & Tousi, A. M. (2018) Experimental Investigation of Inlet Distortion Effect on Performance of a Micro Gas Turbine. Journal of Engineering for Gas Turbines and Power, 140(9).

Pecinka, J., Bugajski, G. T., Jilek, A. & Kmoch, P. (2015) Small engine inlet distortion testing device, 2015 International Conference on Military Technologies (ICMT).

Reid, C. (1969) The Response of Axial Flow Compressors to Intake Flow Distortion, ASME 1969 Gas Turbine Conference and Products Show. V001T01A029.

Turner, M. G., Reed, J. A., Ryder, R. & Veres, J. P. (2004) Multi-Fidelity Simulation of a Turbofan Engine With Results Zoomed Into Mini-Maps for a Zero-D Cycle Simulation, ASME Turbo Expo 2004: Power for Land, Sea, and Air.

Teixeira, M., Romagnosi, L., Mezine, M., Baux, Y., Anker, J., Claramunt, K. & Hirsch, C. (2018) A Methodology for Fully-Coupled CFD Engine Simulations, Applied to a Micro Gas Turbine Engine, ASME Turbo Expo 2018: Turbomachinery Technical Conference and Exposition. V02CT42A047.

Wang, F. (2013) *Whole aero-engine meshing and CFD simulation*. Ph.D. Imperial College London.

Westbrook, C. K. & Dryer, F. L. (1984) Chemical kinetic modeling of hydrocarbon combustion. Progress in Energy & Combustion Science, 10(1), 1-57.

Yan, W., Hu, J., Tu, B. F., Zhang, C. K. & Yin, C. (2015) Analytical model of inlet distortion effect on aerodynamic stability of variable cycle engine. Journal of Aerospace Power, 30(11), 2680-2687.